Nanomechanical Quantification of Elastic, Plastic, and Fracture Properties of $LiCoO_2$

*Meng Qu, William H. Woodford, John M. Maloney, W. Craig Carter, Yet-Ming Chiang, and Krystyn J. Van Vliet**

$LiCoO_2$ is an important lithium storage compound that adopts a distorted rock-salt structure of the α-$NaFeO_2$ type. After the discovery of reversible lithium (de)intercalation in this layered host compound by Mizushima et al.,[1] this material became central to the introduction and subsequent development of lithium-ion batteries (LIBs) of high energy and power density. The advantages of $LiCoO_2$ as a lithium-ion positive electrode material are numerous and include high specific capacity and energy density,[1] high electronic[2] and ionic[3–5] conductivities, long cycle life,[6] and relatively modest structural distortion with varying lithium concentration.[7] A broad range of isostructural compositions within the pseudoquaternary system Li(Co,Ni,Mn,Al)O_2 remain at the forefront of lithium battery research and development.[8]

Despite the relatively modest structural distortion induced by electrochemical cycling (≈1.9 vol%),[7] $LiCoO_2$-type active particles experience heavy mechanical damage after a modest number of electrochemical cycles. Fractured particles and large dislocation densities have been observed in transmission electron microscopy (TEM) studies of $LiCoO_2$,[9–11] $LiAl_{0.25}Co_{0.75}O_2$,[11] and $LiNi_{1/3}Mn_{1/3}Co_{1/3}O_2$.[12] We have previously described this phenomenon of electrochemical cycling-induced fracture as electrochemical shock, due to the close analogy with thermal shock of brittle materials.[13] Electrochemical shock has been demonstrated to correlate with impedance growth and capacity fade in lithium-ion batteries.[14]

Following initial work by Huggins and Nix,[15] there have been many recent analytical and numerical studies aimed at identifying operating conditions, materials, and/or microstructures that prevent or limit electrochemical shock.[13,16–23] Experimentally measured elastic and fracture properties are essential to enable the use of these models as battery engineering tools. $LiCoO_2$ is a model system to study the mechanical behavior of lithium-storage compounds, and is widely used in both materials research and industrial LIB applications. However, the mechanical properties of $LiCoO_2$ are still not well established. For example, there exists a wide range of Young's elastic moduli E reported from both experiments and simulations. Wang et al.[24] reported the bulk elastic modulus B of $LiCoO_2$ as 149 ± 2 GPa from high-pressure synchrotron X-ray powder diffraction (XRD) experiments; this value was corroborated by density functional theory (DFT) calculations in the local density approximation (LDA) and generalized gradient approximation (GGA) with calculated bulk moduli of 168.5 and 142.9 GPa, respectively. Hart and Bates[25] used an atomistic empirical potential model to estimate the anisotropic elastic constants of single crystals; these estimates give the Young's elastic modulus $E = s_{11}^{-1}$ in the range 315–516 GPa, depending on crystallographic orientation. Finally, Kramer and Ceder[26] calculated the equilibrium surface energies of several $LiCoO_2$ surfaces by DFT with the GGA+U exchange correlation functional; this relates to fracture resistance, as the energy required of bond cleavage along fracture planes depends generally on the magnitude of surface energy. To the best of our knowledge, experimental measurements of fracture toughness for $LiCoO_2$ have not been reported previously.

Here, we measured the Young's elastic modulus E, hardness H, and fracture toughness K_{Ic} of individual grains in polycrystalline $LiCoO_2$ (**Figure 1**a) via instrumented nanoindentation.[27–34] These experiments were conducted on dense, sintered polycrystalline compacts of 100 μm average grain diameter, such that the strain volume of indentation was small compared to grain volume. This sample format and grain size gave access to mechanical properties reasonably interpreted as those of a single grain, and also enabled acquisition of several replicate experiments within each grain. To quantify K_{Ic}, we calibrated and implemented the pop-in method by which large probe displacements are related to fracture events (Figure 1b). This provided an efficient way to determine the critical stress intensity factor (hereafter, fracture toughness) K_{Ic} directly from instrumented nanoindentation load-displacement responses without the requirement of direct imaging of each indentation to estimate crack length. We compared the crack length from the pop-in method with the direct imaging method, the latter achieved via atomic force microscopy (AFM) imaging (**Figure 2**), and obtained comparable results.[27,35,36] Finally, we considered the possibility of crystallographic anisotropy as a source of the grain-to-grain variations in K_{Ic} by examining a preliminary correlation with grain orientation.

The measured E obtained on 21 individual grains of polycrystalline $LiCoO_2$ was 174 GPa ± 25 GPa (mean ± standard deviation). This magnitude ranged from 151–236 GPa among all replicate measurements, with a coefficient of variation (standard deviation/mean ≈14%) that is typical for elastic moduli of crystals as determined via nanoindentation. Average hardness of these individual grains was H = 11.7 ± 3.8 GPa. At this maximum indentation load (2 mN), there was no detectable crack

Dr. M. Qu, Dr. W. H. Woodford, Dr. J. M. Maloney, Prof. W. C. Carter, Prof. Y.-M. Chiang, Prof. K. J. Van Vliet
Department of Materials Science and Engineering
Massachusetts Institute of Technology
Cambridge, MA 02139, USA
E-mail: krystyn@mit.edu

DOI: 10.1002/aenm.201200107

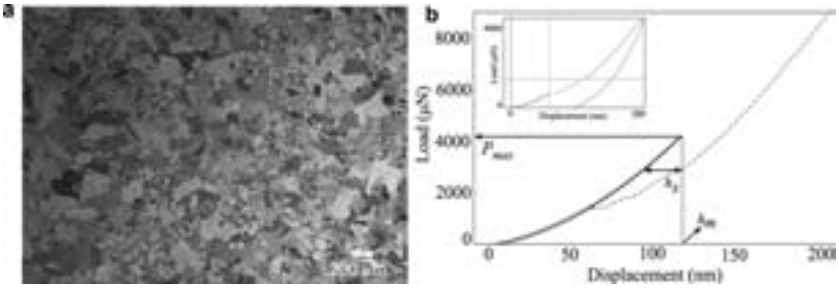

Figure 1. a) Optical micrograph indicating average grain diameter of $LiCoO_2$ > 100 μm. b) Load-displacement data acquired within individual grains indicates displacement bursts or pop-ins that are indicative of fracture events. Below the fracture threshold, these data provide access to the elastic modulus and hardness of each grain. Beyond this threshold, curve fitting to calculate h_x and h_m provides direct access to fracture toughness, K_{Ic} (see Experimental Section).

formation. This measured elastic modulus is comparable to the only other experimentally measured value of elastic modulus for $LiCoO_2$ powder ($E \approx 171$ GPa); this value of Young's elastic modulus was calculated from the reported bulk elastic modulus B (and assumed Poisson's ratio $\nu = 0.3$), which was obtained from high-pressure synchrotron XRD experiments.[24] Although Poisson's ratio has not been measured directly for these materials, ν for similar metal oxides ranges 0.2–0.3.[37] We note that the elastic moduli extrapolated from XRD and measured in the present work are considerably lower than what is indicated by the atomistic model of Hart and Bates[25] (E = 315–516 GPa). That model was based on an empirical potential that was benchmarked against only the unit cell parameters, and the calculated elastic moduli are apparently overestimated as compared to ab initio calculations, estimations from XRD,[24] and our direct measurements.

In these same grains, indentations of higher maximum load (up to 9 mN) were conducted to induce cracking. The measured modulus E and hardness H (at P_{max} = 2 mN) corresponding to each individual grain were used to calculate the fracture toughness K_{Ic} in that grain. AFM images were acquired on the indentations in each individual grain (Figure 2a). These images revealed that some indentations near or on sintered grain boundaries were larger than the indentations located well within the grains; this suggests that, as expected, these sintered grain boundaries were weaker than the grain interior. While it is interesting and important to characterize intergranular fracture toughness for certain cathode formats, we presently seek to determine the transgranular or single-crystal fracture toughness. To analyze K_{Ic} of the grains, only indentations located more than 5 μm away from the grain boundaries visible on the surface were considered further. **Figure 3**a shows the fracture toughness K_{Ic} measured among these grains, which ranged from 0.2 ± 0.02 (arithmetic mean ± standard error) to 6.5 ± 0.7 MPa $m^{1/2}$, with an average K_{Ic} = 1.7 ± 0.4 MPa $m^{1/2}$ and a median value of K_{Ic} = 0.9 ± 0.4 MPa $m^{1/2}$. Two-thirds of the measured grains (14 out of 21) exhibited K_{Ic} less than 1.1 MPa $m^{1/2}$, with a mean value among that population of grains of 0.6 ± 0.1 MPa $m^{1/2}$. Another four grains exhibited an average K_{Ic} of 2.5 ± 0.1 MPa $m^{1/2}$, and three grains exhibited K_{Ic} exceeding 4 MPa $m^{1/2}$. This indicates a wide distribution of fracture toughness among the different grains, with high repeatability of measurements within each grain.

The present measured average fracture toughness for $LiCoO_2$ is in agreement with crystal chemical expectations for a transition metal oxide based on a close-packed oxygen anion sublattice. Absent R-curve effects that modulate fracture toughness (e.g., crack deflection, bridging, transformation toughening, etc.) similar materials typically exhibit K_{Ic} in the range 1–4 MPa $m^{1/2}$.[38–40] We expect that the range in the present fracture toughness data is in part due to crystallographic anisotropy. In magnesium aluminate spinel ($MgAl_2O_4$), crystallographic anisotropy results in a range of measured fracture toughness spanning 1.2–1.9 MPa $m^{1/2}$.[41] In single-crystal sapphire (α-Al_2O_3), the range is 2.4–4.5 MPa $m^{1/2}$.[42] Combining the surface energy data of Kramer and Ceder[43] with the anisotropic elastic data of Hart and Bates,[25] we estimate a factor of two disparity between the maximum and minimum cleavage plane fracture toughnesses in $LiCoO_2$. Residual thermal stresses from cooling of the sintered sample may also broaden the range of measured fracture toughness. Tensile and compressive residual thermal stresses, which are expected from the processing of other oxides of noncubic symmetry,[44] will respectively promote and suppress crack growth during indentation. We believe that the lowest (≈0.2 MPa $m^{1/2}$) and highest (≈6.5 MPa $m^{1/2}$) values reported here are likely influenced by residual stresses. To our knowledge, the thermal expansion asymmetries and residual stress magnitudes of $LiCoO_2$ have not yet been reported.

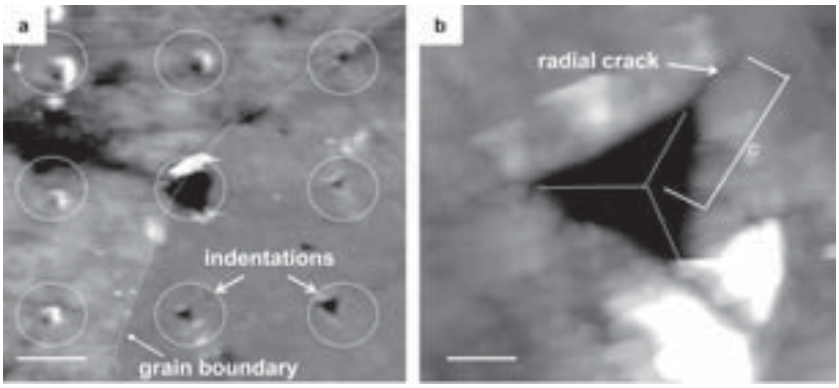

Figure 2. a) Atomic force microscopy contact-mode imaging of nanoindentation grid spanning two adjacent $LiCoO_2$ grains. Scale bar = 5 μm. b) Measuring crack length c' via the direct imaging method enabled validation of the pop-in method of fracture toughness calculation for higher throughput and statistical analysis. Scale bar = 0.5 μm.

To evaluate the reliability of the pop-in method of fracture toughness estimation, we measured the radial crack length of

Adv. Energy Mater. **2012**,
DOI: 10.1002/aenm.201200107

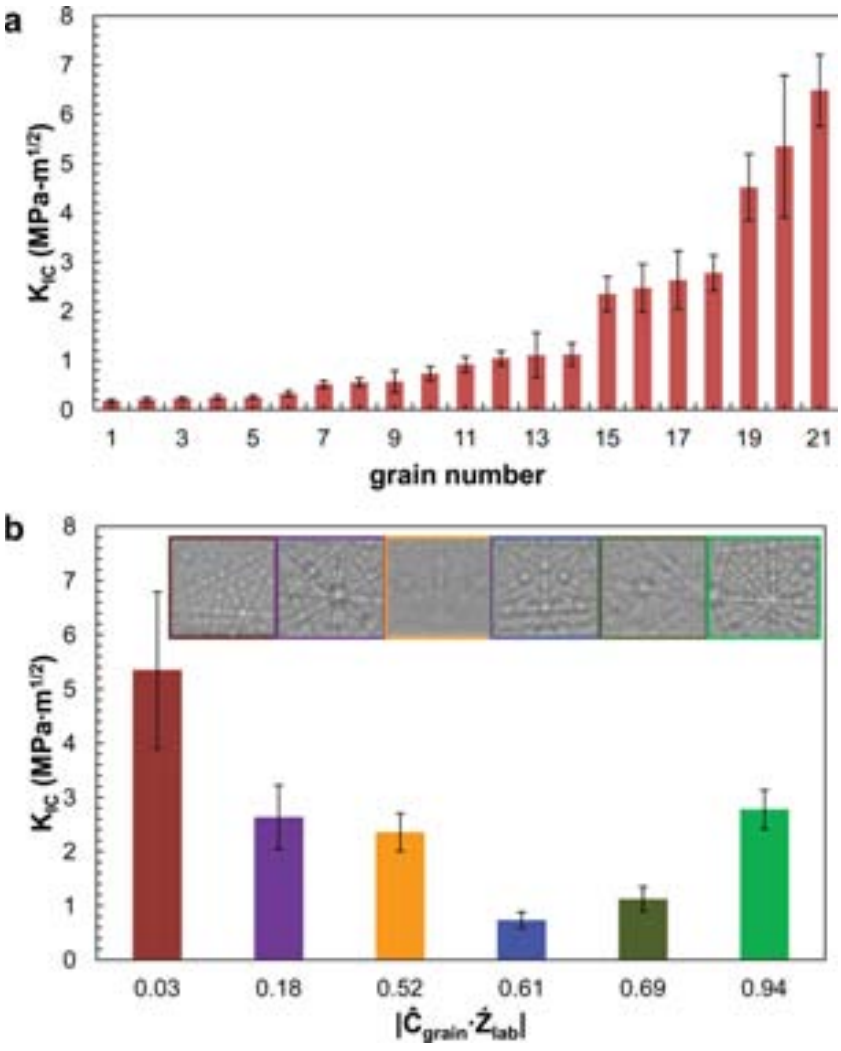

Figure 3. a) Fracture toughness K_{Ic} calculated via the pop-in method. b) K_{Ic} as a function of grain orientation, measured by electron backscatter diffraction and quantified by a grain misorientation metric. No statistically significant correlation was identified between fracture toughness and grain orientation. The inset images are the area diffraction patterns used to index the crystallographic orientation of the corresponding grain.

the indents in two individual grains using the direct-imaging method (see Experimental Section). The crack tip was imaged carefully by using the line trace in each AFM topography image (Figure 2b). The measured average crack lengths c' of the two grains shown in Figure 3b were 720 ± 52 nm and 1231 ± 59 nm. These measured crack lengths are slightly smaller, although still comparable to, the crack lengths c calculated via Equation 5 (791 ± 77.5 nm and 1571 ± 372 nm). This good agreement between methods to estimate the key crack length parameter is encouraging, in that the direct-imaging method requires very time-consuming AFM imaging of each individual indentation, as well as subjective estimation of the crack length based on image analysis. Thus, the pop-in method provides an efficient and reliable approach to measure the crack length and calculate the fracture toughness without requiring post-indentation imaging. Further, others have noted that the direct-imaging method may tend to overestimate the real crack length, which then leads to an underestimation of the fracture toughness.[34] Thus, the pop-in method may also provide a more accurate estimation of K_{Ic} as compared to the direct-imaging method.

The layered structure of $LiCoO_2$ invites the expectation of crystallographically anisotropic properties. The tensor elastic properties of $LiCoO_2$ estimated by atomistic modeling reflect this expected anisotropy.[25] To determine whether there exists a correlation between K_{Ic} and crystal orientation, we measure the orientation of six individual grains using electron backscatter diffraction or EBSD (see Experimental Section). The grain misorientation relative to a laboratory reference is reduced to a scalar metric by taking the absolute value of the dot product between the unit vector along the crystallographic c-axis direction and the sample surface normal unit vector ($|\hat{c}_{grain} \cdot \hat{z}_{lab}|$). Figure 3b shows variation of K_{Ic} with this grain orientation metric for these six grains. The collected EBSD pattern of each grain is shown in the inset of Figure 3b, with corresponding colors. The data shown in Figure 3b suggest a minimized fracture toughness K_{Ic} might exist at $|\hat{c}_{grain} \cdot \hat{z}_{lab}| \approx 0.6$–$0.7$. However, further experiments are required to statistically confirm this correlation. This is due to the low sample set n in the current comparison. Here n is the number of grains that were tested for both K_{Ic} and grain misorientation ($n = 6$), and reflects the challenge of acquiring nanomechanical and diffraction data on the same grains. This low n value limits conclusions on statistically significant differences. That is, although the current data suggested an alternate hypothesis of minimized fracture toughness near $|\hat{c}_{grain} \cdot \hat{z}_{lab}| \approx 0.6$–$0.7$, the p-value of these test is $p = 0.26$, which is significantly higher than $p = 0.05$ (95% confidence for significant difference). Thus, the evaluation of this hypothesis awaits further experimental data. At present, no statistically significant conclusion can be drawn to indicate a correlation between K_{Ic} and crystal orientation. Further experiments require careful mapping of the grain orientation using EBSD, as well as measuring the fracture toughness in each individual grain. As our goals in this paper were to measure E and K_{Ic} within different grains of polycrystalline $LiCoO_2$, and to quantify potential differences in these mechanical properties among grains, detailed correlations between crystallographic orientation and fracture toughness are beyond the scope of the present study.

In conclusion, we report the Young's elastic modulus, hardness, and fracture toughness of $LiCoO_2$, all obtained directly by measuring the indentation response of individual grains in sintered compacts of polycrystalline $LiCoO_2$. We compared two methods to calculate fracture toughness K_{IC} based on nanoscale measurements of crack extension and found these to be

comparable, enabling many replicate experiments within and among grains via the more expedient method. K_{Ic} varied over an order of magnitude among $LiCoO_2$ grains, with a mean and median fracture toughness of 1.7 ± 0.4 MPa-m$^{1/2}$ and 0.9 ± 0.4 MPa-m$^{1/2}$, respectively. Although we considered possible correlations between fracture toughness K_{IC} and crystal orientation, no conclusive correlations were identified. These experimentally measured elastic, plastic, and fracture properties can serve as useful input for the modeling of electrochemical–mechanical coupling in $LiCoO_2$, and also inform the design of operating conditions and microstructures that limit or prevent mechanical damage during electrochemical cycling of lithium-ion batteries. Further, we anticipate that the experimental methods demonstrated herein can be applied to study the elastic and fracture properties of isolated LIB particles and of other dense ceramics, including but not limited those under development for energy storage applications.

Experimental Section

Sample Preparation: Two dense $LiCoO_2$ ceramic pellets were prepared from commercial, battery-grade $LiCoO_2$ powder (AGC Seimi Chemical Co. Ltd, Kanagawa, Japan) by pressing ≈1.8 g of powder into a die (0.5 inches (1 inch ≈ 2.54 cm) diameter) under an applied uniaxial compressive stress of 100 MPa. Pellets were sintered at 1060 °C for 8 h with a heating rate of 9 °C min^{-1} and furnace cooled, yielding an approximate grain diameter of 10 µm. To coarsen the grains, the samples were fired a second time at 1100 °C for 12 h with the same heating and cooling rates. Optical microscopy showed that the average grain diameter in the coarsened samples exceeded 100 µm (Figure 1a). The density of the pellets was found to be 4.80 g cm^{-3} (96% relative density), as determined by Archimedes' method in isopropanol; this measurement was repeated three times for each sample. Coarsened samples were polished using silicon carbide sandpaper of decreasing grits (500, 1200, and 4000) and diamond polishing pads (UltraPrep, Buehler Limited, Lake Bluff, IL); grit sizes of 3 and 1 µm were used for the final polishing steps to achieve a mirror-like finish on the $LiCoO_2$ surface. Samples were cleaned with ethanol between each polishing step and additionally with acetone between final polishing and measurement.

Measurement of E, H, and K_{IC}: The Young's elastic moduli E of 21 individual grains from two identical samples were determined via instrumented nanoindentation (TriboIndenter, Hysitron, Inc., Minneapolis, MN). Thirty indentations were conducted on each individual grain, with an integrated optical microscope enabling placement of an indentation grid in each grain that was distant from grain boundaries. A Berkovich diamond indenter (probe semiapex angle = 65.3°) was used to achieve maximum indentation loads P_{max} of 2 mN. The continuity of the load-displacement responses indicated that there was no detectable crack formation at this maximum load. Loading and unloading times were 10 s, with a 10 s dwell period at maximum load. The center-to-center indentation spacing was 10 µm, which was large compared to the typical maximum indentation depth of 100 nm. Reduced elastic moduli (E_r) were calculated as[45,46]

$$E_r = \frac{dP}{dh}\frac{1}{2h_p}\frac{1}{\beta}\sqrt{\frac{\pi}{24.5}} \quad (1)$$

where h_p is the calculated contact indentation depth and the geometric constant β = 1.034 for the Berkovich pyramid. The Young's elastic modulus of the sample E was calculated from E_r as

$$\frac{1}{E_r} = \frac{1-\upsilon^2}{E} + \frac{1-\upsilon_i^2}{E_i} \quad (2)$$

assuming the Young's modulus and Poisson's ratio of the diamond probe to be E_i = 1070 GPa and ν_i = 0.07, respectively; we assumed ν = 0.3 for $LiCoO_2$. Hardness H was calculated using Equation 3[45,46]

$$H = \frac{p_{max}}{A} \quad (3)$$

where A is the contact area at the maximum indentation load P_{max}. The measured elastic modulus E and hardness H that were determined at a maximum load of 2 mN were used to calculate K_{Ic} at higher maximum loads (3–9 mN), since cracking beneath the indenter occurred at those higher loads as required to extract K_{Ic}.

A second series of indentations with intended maximum loads P_{max} of 9 mN was used to measure the fracture toughness in the same grains. Center-to-center indentation spacing was 20 µm, which was again large compared to typical maximum indentation depths of 250 nm. The load at which large displacements (so-called "pop-ins") occurred varied among individual load-depth responses, and thus the load used to calculate K_{Ic} for each indentation varied from 3–9 mN. K_{Ic} was calculated using the pop-in method proposed by Field et al. as[31,32]

$$K_{IC} = k\left(\frac{E}{H}\right)^{1/2}\left(\frac{p}{c^{3/2}}\right) \quad (4)$$

where k is a constant of 0.036 for the conditions of this study,[29,31,32] and c is the crack length calculated from

$$c = \sqrt{2}h_m + \left(Q\frac{E}{H} - \sqrt{2}\right)h_x \quad (5)$$

where Q is a material-independent constant of 4.55.[31] The displacements h_m and h_x were determined by fitting the load-displacement responses at so-called pop-ins (displacement bursts indicating putative fracture events), as described by Field et al.[31] The curve fitting procedure used to estimate h_m and h_x is illustrated in Figure 1b, and was conducted using a custom *Mathematica* 7.0 (Wolfram) code. This method has been validated to calculate the fracture toughness of brittle materials for which pop-ins are associated with the development of radial or median cracks. Postindentation AFM topography images were acquired to locate the grains and indentations; contact mode imaging was conducted on the MFP-3D AFM (Asylum Research, Inc., Santa Barbara, CA). Any indentations that were located close to any pores/surface defects and were less than 5 µm away from the grain boundaries were excluded from further analysis. Therefore, although 30 indentation experiments were conducted on each grain, only 12–16 indentations were used to calculate K_{Ic} for each grain. Figure 3a shows an AFM image for a 3 × 3 array of indentations on two adjacent grains.

To compare the pop-in method of K_{Ic} estimation with that obtained from direct measurement of surface crack length, AFM topography images were also acquired for a subset of these indentations; radial crack length c' was measured directly (Figure 3b). The crack length was obtained by carefully tracing the crack tip from the center of the indentation. The measured crack length c' was compared to the crack length c calculated using Equation 5.

EBSD Measurement of Grain Orientation: Electron backscatter diffraction (EBSD) was performed to study possible effects of crystal anisotropy of fracture toughness in $LiCoO_2$ by comparing measured K_{Ic} values with grain orientation. EBSD measurements were made on a Helios Nanolab 600 with HKL Flamenco software. Background correction was collected at 60 ms/frame with a 64 frame static background over a 400 µm × 400 µm area. Patterns were collected at a 70° incidence (52° from stage, 18° tilt). The diffraction patterns were binned in a 4 × 4 scheme using a 20 kV accelerating voltage, 10 mm working distance and 1.5 nA beam power. EBSD patterns were indexed using $LiCoO_2$ crystallographic data from literature.[47] The space group R-*3m* (SG#166) was used in the hexagonal setting. The lattice parameters are a = 2.8166 Å. c = 14.045 Å and the Wyckoff positions are Li @ 3a (0, 0, 0), Co @ 3b (0, 0, 1/2), O @ 6c (0, 0, 0.26).

The measured Euler angles for each grain (reported according to the Bunge convention) were used to calculate the angular grain misorientation

Adv. Energy Mater. **2012**,
DOI: 10.1002/aenm.201200107

of the crystallographic *c*-axis (threefold symmetry direction) relative to the sample surface normal. We use the absolute value of the dot product between the unit vector along the crystallographic *c*-axis direction and the sample surface normal unit vector ($|\hat{c}_{grain} \cdot \hat{z}_{lab}|$) as a scalar metric for the grain misorientation. While the crystallographic point group symmetry of $LiCoO_2$ does not require elastic isotropy in the *a*–*b* plane, atomistic calculations of the elastic properties show negligible anisotropy in the *a*–*b* plane.[25] Therefore, we expect that the *c*-axis misorientation is most significant in determining the anisotropic mechanical behavior of individual grains. When the misorientation dot product is equal to one, the c-axis is normal to the sample surface; when this quantity is zero, the *c*-axis lies in the plane of the sample surface.

Acknowledgements

M.Q. and W.H.W. contributed equally to this work, and thank S. Chen of the NSF-supported MIT MRSEC Center for Materials Science and Engineering for assistance with EBSD. We acknowledge support from the US Department of Energy Basic Energy Sciences Small Group Research Program (J. Vetrano, Program Officer). K.J.V.V. also acknowledges support from the Presidential Early Career Award in Science & Engineering (PECASE) administered by the US Air Force Office of Scientific Research.

Received: February 11, 2012
Published online:

[1] K. Mizushima, P. C. Jones, P. J. Wiseman, J. B. Goodenough, *Mater. Res. Bull.* **1980**, *15*, 783.
[2] J. Molenda, A. Stoklosa, T. Bak, *Solid State Ionics* **1989**, *36*, 53.
[3] M. D. Levi, G. Salitra, B. Markovsky, H. Teller, D. Aurbach, U. Heider, L. Heider, *J. Electrochem. Soc.* **1999**, *146*, 1279.
[4] A. Van der Ven, G. Ceder, *Electrochem. Solid-State Lett.* **2000**, *3*, 301.
[5] Y.-I. Jang, B. J. Neudecker, N. J. Dudney, *Electrochem. Solid-State Lett.* **2001**, *4*, A74.
[6] Z. Chen, J. R. Dahn, *Electrochim. Acta* **2004**, *49*, 1079.
[7] J. N. Reimers, J. R. Dahn, *J. Electrochem. Soc.* **1992**, *139*, 2091.
[8] B. Ellis, K. T. Lee, L. F. Nazar, *Chem. Mater.* **2010**, *22*, 691.
[9] H. Gabrisch, R. Yazami, B. Fultz, *Electrochem. Solid-State Lett.* **2002**, *5*, A111.
[10] H. Gabrisch, R. Yazami, B. Fultz, *J. Power Sources.* **2003**, *119–121*, 674.
[11] H. Wang, Y.-I. Jang, B. Huang, D. R. Sadoway, Y.-M. Chiang, *J. Electrochem. Soc.* **1999**, *146*, 473.
[12] H. Gabrisch, T. Yi, R. Yazami, *Electrochem. Solid-State Lett.* **2008**, *11*, A119.
[13] W. H. Woodford, Y.-M. Chiang, W. C. Carter, *J. Electrochem. Soc.* **2010**, *157*, A1052.
[14] Y. Itou, Y. Ukyo, *J. Power Sources.* **2005**, *146*, 39.
[15] R. A. Huggins, W. D. Nix, *Ionics.* **2000**, *6*, 57.
[16] T. Maxisch, G. Ceder, *Phys. Rev. B: Condens. Matter* **2006**, *73*, 174112.
[17] J. Li, A. K. Dozier, Y. Li, F. Yang, Y.-T. Cheng, *J. Electrochem. Soc.* **2011**, *158*, A689.
[18] Y.-T. Cheng, M. W. Verbrugge, *J. Electrochem. Soc.* **2010**, *157*, A508.
[19] Y. Hu, X. Zhao, Z. Suo, *J. Mater. Res.* **2010**, *25*, 1007.
[20] Y.-T. Cheng, M. W. Verbrugge, *Electrochem. Solid-State Lett.* **2010**, *13*, A128.
[21] T. K. Bhandakkar, H. Gao, *Int. J. Solid. Struct.* **2010**, *47*, 1424.
[22] K. Zhao, M. Pharr, J. J. Vlassak, Z. Suo, *J. Appl. Phys.* **2010**, *108*, 075517.
[23] R. Grantab, V. B. Shenoy, *J. Electrochem. Soc.* **2011**, *158*, A948.
[24] X. Wang, I. Loa, K. Kunc, K. Syassen, M. Amboage, *Phys. Rev. B: Condens. Matter* **2005**, *72*, 224102.
[25] F. X. Hart, J. B. Bates, *J. Appl. Phys.* **1998**, *83*, 7560.
[26] D. Kramer, G. Ceder, *Chem. Mater.* **2009**, *21*, 3799.
[27] G. R. Anstis, P. Chantikul, B. R. Lawn, D. B. Marshall, *J. Am. Ceram. Soc.* **1981**, *64*, 533.
[28] B. R. Lawn, A. G. Evans, D. B. Marshall, *J. Am. Ceram. Soc.* **1980**, *63*, 574.
[29] D. S. Harding, W. C. Oliver, G. M. Pharr, in *Materials Research Society Proceedings* (Eds: S. P. Baker, P. Børgesen, C. A. Ross, P. H. Townsend, C. A. Volkert), Vol. *356*, Materials Research Soc., Pittsburgh, USA **1994**, p. 663.
[30] G. M. Pharr, D. S. Harding, W. C. Oliver, in *NATO ASI Series, Series E: Applied Science* (Eds: M. Nastasi, D. M. Parkin, H. Gleiter), Vol. *233*, Kluwer Academic Publishers, Dordrecht, The Netherlands **1993.**
[31] J. S. Field, M. V. Swain, R. D. Dukino, *J. Mater. Res.* **2003**, *18*, 1412.
[32] T. Scholz, G. A. Schneider, J. Munoz-Saldana, M. V. Swain, *Appl. Phys. Lett.* **2004**, *84*, 3055.
[33] M. T. Laugier, *Mater. Sci. Lett.* **1987**, *6*, 355.
[34] R. Li, L. Bao, X. Li, *CrystEngComm* **2011**, *13*, 5858.
[35] J. Alvarado-Rivera, J. Munoz-Saldana, R. Ramirez-Bon, *Thin Solid Films* **2011**, *519*, 5528.
[36] Z. Burghard, A. Zimmermann, J. Rodel, F. Aldinger, B. R. Lawn, *Acta Mater.* **2004**, *52*, 293.
[37] *CRC Materials Science and Engineering Handbook*, 3rd ed. (Eds: J. F. Shackelford, W. Alexander), CRC Press, Boca Raton, USA **2000.**
[38] D. L. Whitney, M. Broz, R. F. Cook, *Am. Mineral.* **2007**, *92*, 281.
[39] B. Lawn, *Fracture of Brittle Solids*, 2nd ed., Cambridge University Press, Cambridge, UK **1993.**
[40] G. R. Anstis, P. Chantikul, B. R. Lawn, D. B. Marshall, *J. Am. Ceram. Soc.* **1981**, *64*, 533.
[41] R. L. Stewart, R. C. Bradt, *J. Mater. Res.* **1980**, *15*, 67.
[42] M. Iwasa, R. C. Bradt, *Adv. Ceram.* **1984**, *10*, 767.
[43] D. Kramer, G. Ceder, *Chem. Mater.* **2009**, *21*, 3799.
[44] Q. Ma, D. R. Clarke, *J. Am. Ceram. Soc.* **1994**, *77*, 298.
[45] G. M. Pharr, W. C. Oliver, F. R. Brotzen, *J. Mater. Res.* **1992**, *7*, 613.
[46] A. C. Fischer-Cripps, *Nanoindentation*, Springer, New York **2004.**
[47] W. D. Johnston, R. R. Heikes, D. Sestrich, *J. Phys. Chem. Solids* **1958**, *7*, 1.